ELSEVIER

Contents lists available at ScienceDirect

Journal of Controlled Release

journal homepage: www.elsevier.com/locate/jconrel





Elongated PEO-based nanoparticles bind the high-density lipoprotein (HDL) receptor scavenger receptor class B I (SR-BI)

Mitch Raith ^a, Sarah J. Kauffman ^b, Monireh Asoudeh ^a, Jennifer A. Buczek ^c, Nam-Goo Kang ^d, Jimmy W. Mays ^d, Paul Dalhaimer ^{a,e,*}

- ^a Department of Chemical and Biomolecular Engineering, University of Tennessee, Knoxville, TN 37996, United States of America
- ^b Department of Microbiology, University of Tennessee, Knoxville, TN 37996, United States of America
- ^c College of Veterinary Medicine, University of Tennessee, Knoxville, TN 37996, United States of America
- ^d Department of Chemistry, University of Tennessee, Knoxville, TN 37996, United States of America
- e Department of Biochemistry, Cellular, and Molecular Biology, University of Tennessee, Knoxville, TN 37996, United States of America

ARTICLE INFO

Keywords: Nanoparticle Filomicelle PEG HDL SR-BI SARS-CoV-2

ABSTRACT

Targeting cell-surface receptors with nanoparticles (NPs) is a crucial aspect of nanomedicine. Here, we show that soft, flexible, elongated NPs with poly-ethylene-oxide (PEO) exteriors and poly-butadiene (PBD) interiors – PEO-PBD filomicelles - interact directly with the major high-density lipoprotein (HDL) receptor and SARS-CoV-2 uptake factor, SR-BI. Filomicelles have a \sim 6-fold stronger interaction with reconstituted SR-BI than PEO-PBD spheres. HDL, and the lipid transport inhibitor, BLT-1, both block the uptake of filomicelles by macrophages and Idla7 cells, the latter are constitutively expressing SR-BI (Idla7-SR-BI). Co-injections of HDL and filomicelles into wild-type mice reduced filomicelle signal in the liver and increased filomicelle plasma levels. The same was true with $SCARB1^{-/-}$ mice. SR-BI binding is followed by phagocytosis for filomicelle macrophage entry, but only SR-BI is needed for entry into Idla7-SR-BI cells. PEO-PBD spheres did not interact strongly with SR-BI in the above experiments. The results show elongated PEO-based NPs can bind cells via cooperativity among SR-BI receptors on cell surfaces.

1. Introduction

Given the prevalence of metabolic disorders such as obesity [1], there is great need to target surface receptors on cells that are involved in mammalian-wide lipid and cholesterol homeostasis using nanoparticles (NPs). Lipoproteins play a major role in controlling the distribution of neutral lipids and cholesterol. A subset of lipoproteins – mostly high-density lipoprotein (HDL) - bind scavenger receptor class B I (SR-BI) [2]. HDL transports cholesterol from tissues and delivers it to SR-BI on the liver and on macrophages [3-6]. SR-BI is also an entry point for certain pathogens [7]. Hepatitis C virus uses SR-BI to enter cells [8,9], as does SARS-CoV-2 [10]. These viruses bind HDL, which most likely guides their cellular entry [10,11]. Thus, SR-BI is an attractive NP target for modulating metabolic imbalances and for combating certain pathogen infections. The issue is how to target SR-BI. In theory this can be done by attaching an SR-BI-targeting ligand to the exterior of the NP. However, the mechanistic molecular interactions between HDL and SR-BI are unknown, thus negating the identification of a potential ligand

that can be conjugated to a NP. Alternatively, lipoprotein can be modified and used to deliver drugs. However, this can be expensive and time consuming [12]. A cost-effective and biocompatible approach to targeting this crucial receptor is needed.

Here, we show that soft poly-ethylene-oxide (PEO)ylated NPs (synonymous with poly-ethylene-glycol (PEG)ylated NPs) with poly-butadiene (PBD) cores that are elongated in one dimension – PEO-PBD filomicelles – achieve the above goals with respect to binding SR-BI and being internalized by cells expressing SR-BI. PEO-PBD filomicelles bind reconstituted human SR-BI (rSR-BI) in pull down experiments. PEO-PBD filomicelle uptake by M1 and M2 murine macrophages is blocked by human HDL (hHDL) and by the small blocks-lipid-transport molecule, BLT-1, in co-incubation titration experiments. These results also hold for Idla7 cells constitutively expressing SR-BI (Idla7-SR-BI) cells. PEO-PBD filomicelles increase the expression level of SR-BI in M1 and M2 murine macrophages. *In vivo*, co-injections of PEO-PBD filomicelles and hHDL into wild-type mice resulted in a ~ 2-fold decrease in PEO-PBD filomicelle localization to the liver. This was also true when

^{*} Corresponding author at: Department of Chemical and Biomolecular Engineering, University of Tennessee, Knoxville, TN 37996, United States of America. E-mail address: pdalhaim@utk.edu (P. Dalhaimer).

PEO-PBD filomicelles were injected solitarily into SR-BI-deficient mice (SCARB1^{-/-}). PEO-PBD filomicelle levels in the plasma were increased over controls in both experiments. By using a panel of inhibitors for classic NP entry points into cells, we show that polyinosinic (PI) acid, an SR-BI blocker, negates the uptake of PEO-PBD filomicelles by Idla7-SR-BI cells. PEO-PBD filomicelles enter M1 and M2 murine macrophages by a combination of SR-BI binding and subsequent phagocytosis. In the above experiments, spherical PEO-PBD analogs did not have appreciable interactions with SR-BI. Thus, elongated filomicelles that have a PEO exterior have excellent potential in metabolic applications. These include modulating reverse cholesterol transport by increasing expression levels of SR-BI to increase uptake of HDL, delivering active agents to cells through SR-BI, and blocking SR-BI in certain situations such as foam cell progression. Blocking SR-BI with PEO-PBD filomicelles could also be a strategy for reducing pathogen uptake. Our results point to a new paradigm for binding and entering cells that express SR-BI, a major player in metabolic homeostasis and pathogenesis.

2. Materials and methods

2.1. Nanoparticles

PEO $_{56}$ -PBD $_{46}$ diblock copolymers (filomicelles) were synthesized according to the methods of Ref. 13. PEO $_{132}$ -PBD $_{69}$ diblock copolymers (spheres) were a gift from Dr. Frank S. Bates (Univ. of Minnesota). NPs were formed at 10 mg/ml copolymer using film rehydration with phosphate buffered saline (PBS) as the aqueous buffer as described previously [14]. 50 nm spherical carboxylated polystyrene (PS)-COOH NPs were purchases from Bangs Labs (#PC2002). Nanoparticles were stained with hydrophobic PKH-26/67 or near-infrared (NIR) dyes and dialyzed overnight into PBS [15]. The PBS was changed three times.

2.2. SEM imaging

200 mesh copper grids with a thin carbon film were made to be hydrophilic by placing the grid with film in weak plasma for 30 s. The grid with carbon film was then floated on a small drop of sample for 1 min, excess sample was quickly removed by touching the edge of the grid to a piece of filter paper. The grid with sample was washed with water then stained with 1% uranyl acetate, after 1 min excess stain was removed by touching the edge of the grid to a piece of filter paper. The images were taken by ZEISS LIBRA 200 HT FE and analyzed by ImageJ (Fiji).

2.3. Binding assays

hHDL was purchased from Lee BioSolutions (#361–10). The solution contained 3320 mg/dL total cholesterol, 1350 mg/dL triglyceride, and 3070 hHDL cholesterol. Electrophoresis (Helena QuickGel) preformed at Lee BioSolutions showed one major band corresponding to ApoA-I. PSCOOH NPs were pelleted by centrifugation. Filomicelles were pelleted using immune precipitation. Briefly, filomicelles and hHDL or rSR-BI (R and D systems; #8114-SRB) were mixed for 3 h at 4 °C. An antibody for PEG (Abcam; #ab133471) was then added and the mixed was mixed at 4 °C for an additional hour. Agarose Protein L beads (Santa Cruz Bio; #sc-500,779) were then added for an additional hour. At this point filomicelles with bound Apo-AI were pelleted. The amount of unbound Apo-AI in the supernatant was quantified by spectroscopy (Nanodrop). The amount of Apo-AI bound to the filomicelles and spheres was calculated by subtracting the amount of Apo-AI in the supernatant from the total amount used in the assay.

2.4. Mammalian cell culture

M0 RAW 264.7 macrophages (ATCC; #TIB-71) were polarized into M1-like macrophages by adding 20 ng/ml of IFN- γ (PeproTech;

#315–05) or into M2-like macrophages by adding 10 ng/ml each of IL-4 (PeproTech; #214–14) and IL-13 (PeproTech; #210–13) for 48 h [16]. Increased expression of IL-12 (M1) and IL-10 was confirmed using standard RT-PCR techniques (Fig. S1). Macrophages were maintained at 5% $\rm CO_2$ and 37 $\rm ^{\circ}C$ in DMEM supplemented with 10% FBS and 1% penicillin-streptomycin. Idal7 and Idal7-SR-BI cells were provided by Dr. Monty Krieger (MIT). Idal7 cells were maintained at 5% $\rm CO_2$ and 37 $\rm ^{\circ}C$ in F-12 K supplemented with 10% FBS and 1% penicillin-streptomycin. Idal7-SR-BI also had 200 ng/ml G418 in the media.

2.5. In vitro experiments

18 h prior to experiments, cells were seeded in a 24 well plate. 70–90% confluence was targeted at the start of the experiment. NPs were added to a final concentration of 400 μ g/ml. Plates were swirled to mix. After 2 h, the media was removed, the cells were washed $3\times$ times with PBS and imaged to visualize NP content with an EVOS FL Cell Imaging System (Thermo). Cells were then trypsinized and two volumes of FACSmax (ASMBIO) buffer was added before the cells were aspirated. Cells were then quantitatively analyzed with an Accuri C6 flow cytometer (BD Biosciences). hHDL was added simultaneously with the NPs to the final concentrations stated. Plates were swirled to mix and incubated for 2 h. Analysis was done as described above. The SR-BI-GFP plasma was a gift from Dr. Sergio Grinstein (Univ. of Toronto). SR-A-GFP was in a pcDNA3.1(+)-C-eGFP backbone (Genescript). Inhibitor treatments are described in Table S1.

2.6. SR-BI gene expression assays

M1 and M2 RAW 264.7 macrophages were seeded in a 96 well plate. 70-90% confluence was targeted at the start of the experiment. The described NP or hHDL was added to the culture media for 2 h. NPs were added to a final concentration of 400 $\mu g/ml$ and hHDL to 2.4 mg/ml. After incubation, cells were fixed by adding 1 volume of 10% buffered formalin (Fisher) to each well and incubated for 30 min at 37 $^{\circ}\text{C}$. The cells were then washed 3× with PBS. Blocking and perforation was performed in one step with 10% Goat serum, 0.5%BSA, 0.1%Tween 20 PBS at 37 $^{\circ}\text{C}$ for 1 h. Cell were washed 3× in PBS. 0.5% BSA PBS with $0.5~\mu g/ml$ SR-BI antibody (Novus; #NB400–104) was added and the cells were incubated for 1 h at 37 °C. Cells were washed $3\times$ with PBS before 0.5%BSA PBS containing 1 µg/ml Texas Red conjugated secondary antibody (Abcam; #ab6719) was added. Cells were incubated for 1 h at 37 $^{\circ}$ C. Cells were washed 3× with PBS and switched to PBS containing 100 nM DAPI to counter stain the nucleus for 5 minuets at 23 °C and washed $3\times$ again with PBS. The plate was than analyzed with a VarioSkan LUX (ThermoFisher). Fluorescence was measured both for Texas Red and DAPI. Singly stained wells confirmed there was not significant crosstalk between the channels. The fluorescence of Texas Red was standardized for the number of cells in each well by dividing by the DAPI signal. A gene expression score was assigned by normalizing to the standardized expression of the untreated cells.

2.7. Mouse experiments

All experiments were performed under the guidelines of the University of Tennessee's IACUC protocol #2231. BL6;129S-Scarb1^{m1Kri}/J mice were purchased from Jackson Laboratories and bred in house. Mice were genotyped with tail snip PCR analysis. Litter mates were used as experimental controls. Prior to injection, aggregates that did not form NPs were pelleted at 23 °C for 15 min at 15,000 x g in a Fisher Scientific AccuSpin Micro 17 centrifuge. The upper phase containing the dispersed NPs was reserved for injection although no pellet was visible because the NPs do not appear to form additional aggregates. The upper phase was imaged using SEM. NPs were loaded with 5 µl of a 2.5 mg/ml stock of NIR dye in ethanol for imaging (Life Technologies; #D-12731). The dye partitions into the hydrophobic interiors of the nanoparticles and does

not leak *in vivo* [15]. 100 μ l of 5 mg/ml NP solution in PBS was tail-vein injected into the mice. Mice were euthanized 3 h after injection by isoflurane and cervical dislocation. The HDL plasma concentration of C57BL/6 J mice is reported to be ~0.6 mg/ml [17], correlating to a blood HDL concentration of 0.35 mg/ml. The weight of the mouse was used to calculate the blood volume [18] and the resulting amount of hHDL co-injected with filomicelles. hHDL was injected to reach a level of at least 0.50 mg/ml HDL in the bloodstream to mimic the end point of the *in vitro* titration.

3. Results

We used two types of uncharged PEO-PBD nanoparticles (NPs) in this study: cylindrical/filomicelle and spherical. NP structural details are presented in Fig. 1A-C. Filomicelles and spheres have similar diameters: ~50 nm (Fig. 1D,E). The filomicelles have micron lengths (Fig. 1D)

[13–15]. Both NPs are stable in the cell culture medias used in this study (Fig. 1F-I). We used spherical NPs as controls to determine the effects of NP geometry on NP - SR-BI interactions. Before determining possible interaction between NPs and SR-BI, we first wished to determine if human HDL (hHDL) bound filomicelles. This is a necessary control because HDL could bind a NP and guide it to SR-BI. If this is the case, HDL and not the NP would be responsible for binding SR-BI. We used 50 nm spherical carboxylated polystyrene (PS)-COOH NPs as a positive control because they have micro-molar affinities for hHDL [19]. We incubated PEO-PBD filomicelles and PS-COOH NPs separately with hHDL and determined the amount bound of Apo-AI - the main structural protein of HDL - using gel electrophoresis. Apo-AI bound PS-COOH NPs but did not bind PEO-PBD filomicelles at measurable levels (Fig. 2A). This shows that PEO-PBD filomicelles do not interact with HDL. Therefore, HDL should not be able to bind PEO-PBD filomicelles and guide them to SR-BI. Next, we wished to determine if PEO-PBD NPs

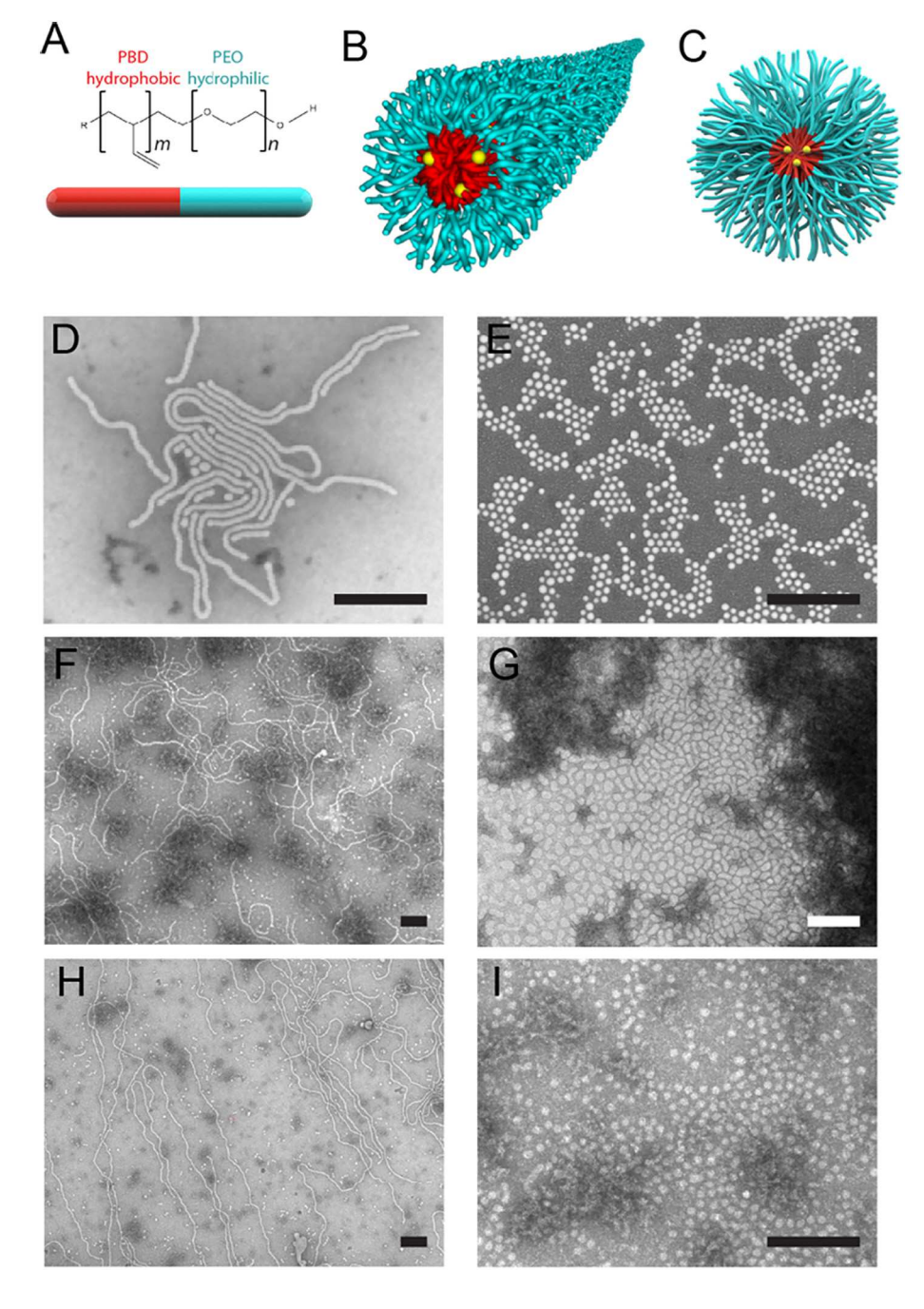


Fig. 1. Properties of PEO-PBD filomicelles and PEO-PBD spheres used in this study. (A) Chemistries of the diblock copolymers. For the filomicelles: m=46, n=56. For the spheres: m=69, n=132. (B—C) Cartoons of a filomicelle (B) and a sphere (C). Yellow spheres represent dye molecules. (D—I) Electron micrographs of filomicelles in PBS (D), spheres in PBS (E), filomicelles in DMEM+FBS + P/S (macrophage media) (F), spheres in DMEM+FBS + P/S (macrophage media) (G), filomicelles in HANKS+FBS + P/S (CHO media) (I). All incubation times were 2 h. Scale bars are 500 nm. (For interpretation of the references to colour in this figure legend, the reader is referred to the web version of this article.)

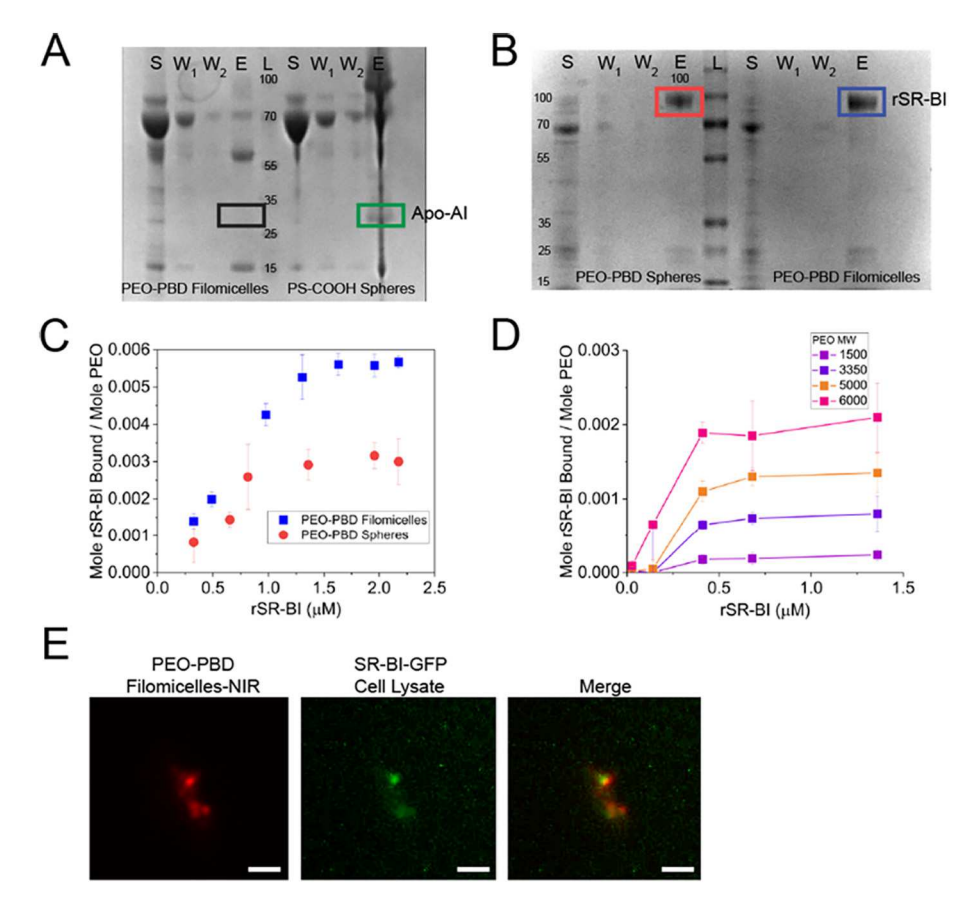


Fig. 2. Binding of PEO-PBD NPs to hHDL and rSR-BI. (A) SDS-Page gel showing the results of a binding experiment where NPs were mixed with hHDL. The major structural protein of HDL, Apo-AI, does not bind PEO-PBD filomicelles (black rectangle). As a positive control we used 50 nm PS-COOH beads as a known binder of Apo-AI (green rectangle). S = supernatant, W = wash, E = elution, L = ladder, (B) SDS-Page gel showing the results of a binding experiment where PEO-PBD spheres (red rectangle) and PEO-PBD filomicelles (blue rectangle) were mixed with recombinant SR-BI (rSR-BI). (C) Plot of the binding of rSB-BI to PEO-PBD filomicelles and PEO-PBD spheres from the experiments described in (B). (D) Plot of the binding of free PEO molecules of varying MW with rSR-BI. (E) Fluorescence micrographs of PEO-PBD filomicelles-NIR that were incubated with lysed Idla7 cells expressing SR-BI-GFP. Scale bars are 5 µm. (For interpretation of the references to colour in this figure legend, the reader is referred to the web version of this article.)

interacted directly with SR-BI. We incubated PEO-PBD filomicelles and PEO-PBD spheres separately with recombinant SR-BI (rSR-BI). The amount of rSR-BI was increased for each experiment to determine how much rSR-BI is needed to saturate either PEO-PBD filomicelles or PEO-PBD spheres. The mixture was allowed to come to equilibrium and the NPs were separated from rSR-BI by centrifugation of micron-size beads covered with an antibody to PEO. The amount of unbound rSR-BI in the supernatant was determined by spectroscopy and the amount of rSR-BI bound to the PEO-PBD NPs was determined by subtraction from the total amount of rSR-BI added to the incubation. PEO-PBD filomicelles pulled down a ~ 3-fold greater amount of rSR-BI than PEO-PBD spheres (Fig. 2B,C). The surface area of one 1 μ m \times 50 nm cylinder/filomicelle is $A = 2\pi rh + 2\pi r^2 \sim 300,000 \text{ nm}^2$. The surface area of one 50 nm sphere is $A = 4\pi r^2 \sim 3000 \text{ nm}^2$. For 20 spheres that compare in length to a 1 µm cylinder, the total surface area $A = 600,000 \text{ nm}^2$, which is twice the exposed surface area of one cylinder. Thus, the difference in the amount of rSR-BI bound can be further increased 2-fold when the available surface areas of the spheres versus the cylinders are taken into account. The lengths of the PEO block of the copolymers are different for the filomicelles (n = 56; ~2500 Da) and the spheres (n = 132; ~5800 Da). To ensure that this PEO length difference was not the reason for different affinities of PEO-PBD filomicelles vs. PEO-PBD spheres for rSR-BI, we performed the above pull-down experiments but with single PEO molecules (not in a NP) of MW 1500, 3350, 5000, and 6000 Da. PEO affinity for rSR-BI increased as a function of PEO length (Fig. 2D). Since the PEO block of the PEO-PBD spheres is longer than the PEO block of the PEO-PBD filomicelles, our NP-rSR-BI binding results are not an artifact of PEO length. Although it must be kept in mind that the conformation of free PEO (coiled) will be different from the conformation of PEO on a NP (brush-like). We wished to determine if PEO-PBD filomicelles localized with SR-BI using fluorescence microscopy. We transfected Chinese Hamster Ovary (CHO) cells that do not express SR-BI (Idla7 cells) with

SR-BI-GFP [2]. We lysed the cells and added PEO-PBD filomicelles carrying near infrared dye (NIR) and added the mixture to a microscope slide. The PEO-PBD filomicelle-NIR and GFP signals overlapped (Fig. 2E). This shows that PEO-PBD filomicelles carrying NIR dye colocalize with SR-BI-GFP after CHO cell lysis. Note that the filomicelle has a short length in the micrograph most likely due to structural disruption caused by cellular factors such as lipids and fatty acids in the lysate.

If PEO-PBD filomicelles bind SR-BI, then HDL could compete for the binding site on the cell surface of an SR-BI-expressing cell. To test this, we set up a series of titrations keeping the amount of filomicelles carrying PKH67 dye (green) at saturating concentrations and increased the amount of unlabeled hHDL in culture with RAW 264.7 M1 and M2 murine macrophages as a model in vitro system because they have high surface expression levels of SR-BI [20]. Also, macrophages are desirable targets in nanomedicine for a wide range of applications. The uptake of filomicelles carrying PKH67 (filomicelles-PKH67) decreased as the concentration of hHDL increased in fluorescence micrographs (Fig. 3A). Fluorescence quantification of the cells by flow cytometry showed a \sim 100-fold drop in signal as the hHDL concentration increased (Fig. 3B; Fig. S2-3). There was no difference in the uptake of spheres carrying PKH67 in the same experiments, except at the highest concentration of hHDL (Fig. 3A,B; Fig. S4-5). We wished to determine if the small molecule BLT-1, which blocks lipid transport at SR-BI [21], also decreased filomicelle uptake by macrophages. BLT-1 lowered the uptake of filomicelles carrying PKH67 in both M1 and M2 murine macrophages by ~10-fold but had no effect on the uptake of spheres carrying PKH67 (Fig. 3C,D; Fig. S6). We used immunofluorescence with SR-BI as the epitope tag to determine the expression levels of SR-BI in M1 and M2 murine macrophages that were incubated with either PBS, hHDL, filomicelles, or spheres for 2 h. SR-BI levels matched for hHDL and filomicelles, and were slightly lower for spheres (Fig. 3E).

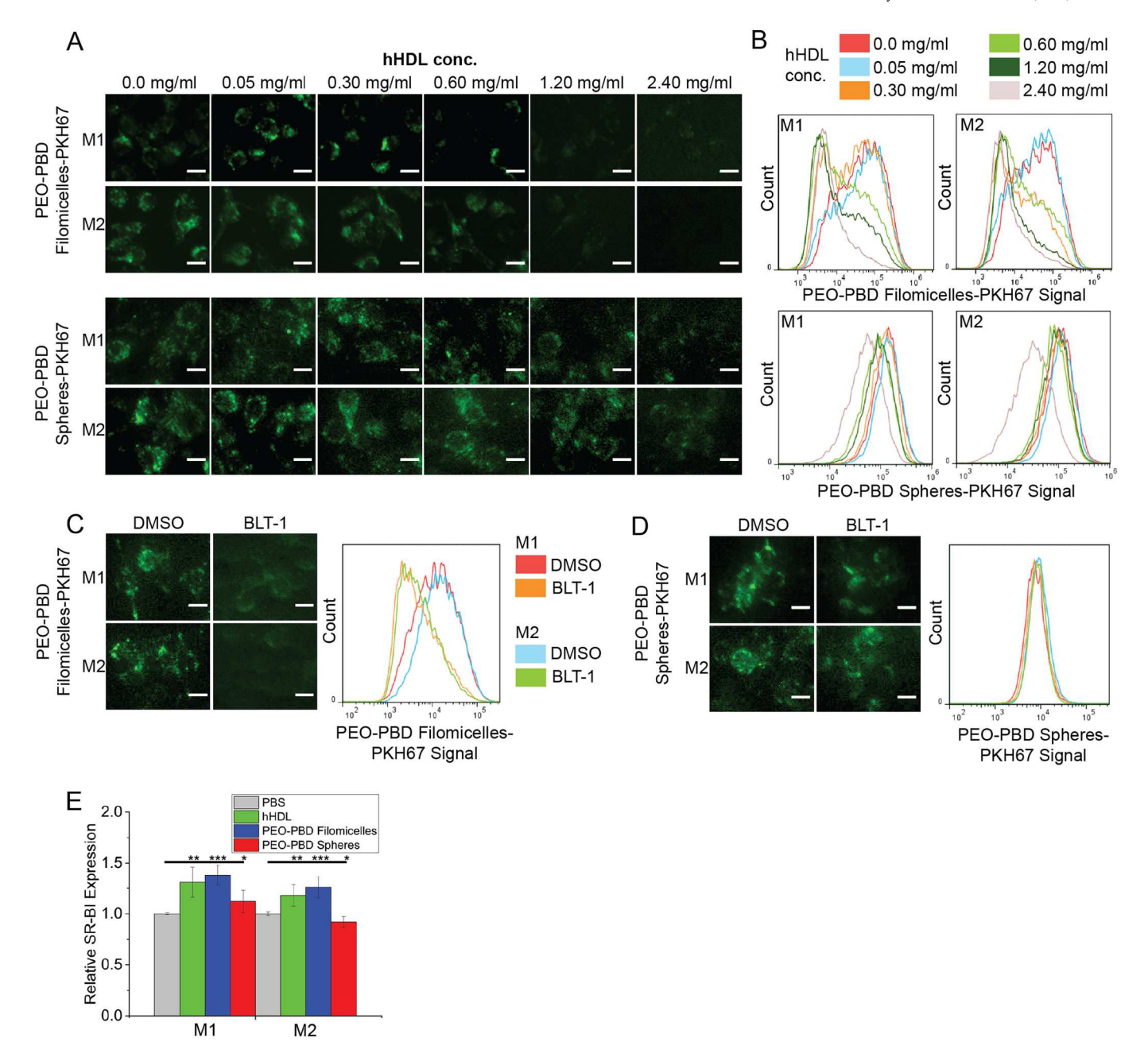


Fig. 3. hHDL and BLT-1 block the uptake of PEO-PBD filomicelles by M1 and M2 murine macrophages. (A) Fluorescence micrographs of M1 and M2 murine macrophages that were incubated with either PEO-PBD filomicelles carrying PKH67 dye or PEO-PBD spheres carrying PKH67 dye and increasing amounts of unlabeled hHDL as indicated. (B) Plots of the fluorescence of the cells shown in (A) measured by flow cytometry. (C) Fluorescence micrographs of M1 and M2 murine macrophages incubated with PEO-PBD filomicelles carrying PKH67 dye in the absence and presence of BLT-1 and accompanying plot of the fluorescence of PEO-PBD filomicelles-PKH67 as measured by flow cytometry. Colour panel is for (C) and (D). (D) Fluorescence micrographs of M1 and M2 murine macrophages incubated with PEO-PBD spheres carrying PKH67 dye in the absence and presence of BLT-1 and accompanying plot of the fluorescence of PEO-PBD spheres-PKH67 as measured by flow cytometry. N = 10 k cells per curve for all plots. All scale bars are 10 µm. (E) Plot of the expression of SR-BI in M1 and M2 murine macrophages as measured by immunofluorescence against SR-BI. Experiments were performed in triplicate. * P < 0.1, ** P < 0.05, *** P < 0.01.

We wished to use a model mammalian cell system that had controllable expression of SR-BI to isolate SR-BI NP uptake from general macrophage NP uptake mechanisms, which are robust. To this end, we used CHO cells that constitutively express SR-BI (Idla7-SR-BI cells) versus CHO cells that do not express SR-BI (Idla7 cells) [22]. We performed similar hHDL titration experiments as the ones described above. As seen in the above experiments with macrophages, hHDL titrations greatly reduced the uptake of PEO-PBD filomicelles carrying PKH67 by Idla7-SR-BI cells (Fig. 4A,B; Fig. S7–8; Movie S1). There was little difference in the uptake of PEO-PBD spheres carrying PKH67 in the same experiments (Fig. 4A,B; Fig. S7–8). No significant uptake difference in

either PEO-PBD filomicelles or PEO-PBD spheres carrying PKH67 was seen in hHDL titration experiments with Idla7 cells (Fig. 4C,D; Fig. S9–10). BLT-1 lowered the uptake of PEO-PBD filomicelles carrying PKH26 by Idla7-SR-BI cells *versus* DMSO controls, but had no difference on PEO-PBD filomicelle uptake by Idla7 cells (Fig. 4E,F; Fig. S11). BLT-1 had no effect on the uptake of PEO-PBD spheres carrying PKH26 by Idla7-SR-BI or Idla7 cells (Fig. 4E,F; Fig. S11). We added an additional conditional SR-BI expression system to our studies to confirm our findings in Idla7-SR-BI cells. We transiently expressed SR-BI-GFP in Idla7 cells and determined the uptake of PEO-PBD filomicelles and PEO-PBD spheres. Idla7 cells expressing SR-BI-GFP had a ~ 4–5-fold higher

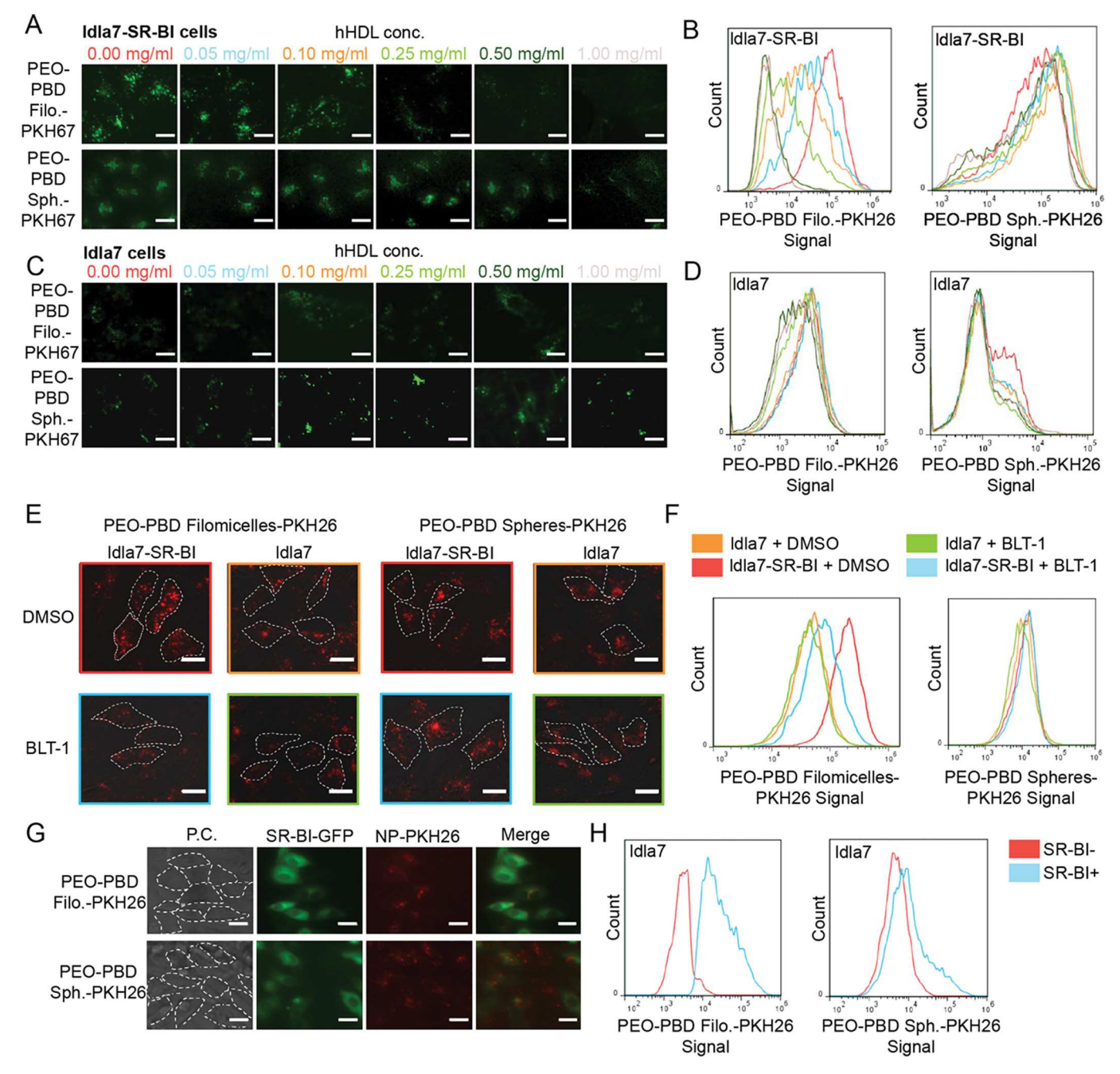


Fig. 4. hHDL and BLT-1 block the uptake of PEO-PBD filomicelles by Idla7-SR-BI cells. (A) Fluorescence micrographs of Idla7-SR-BI cells incubated with PEO-PBD filomicelles carrying PKH67 or PEO-PBD spheres carrying PKH67 with increasing amounts of unlabeled hHDL as indicated. (B) Plots of the fluorescence of the cells shown in (A) measured by flow cytometry. (C) Fluorescence micrographs of Idla7 cells that were incubated with PEO-PBD filomicelles carrying PKH67 or PEO-PBD spheres carrying PKH67 with increasing amounts of unlabeled hHDL as indicated. (D) Plots of the fluorescence of the cells shown in (C) measured by flow cytometry. (E) Fluorescence micrographs of Idla7-SR-BI and Idla7 cells incubated with either PEO-PBD filomicelles carrying PKH26 or PEO-PBD spheres carrying PKH26 and DMSO (control) or BLT-1. (F) Plots of the fluorescence of the cells shown in (E) measured by flow cytometry. (G) Fluorescence micrographs of Idla7 cells that were transfected with SR-BI-GFP and incubated with either PEO-PBD filomicelles carrying PKH26 or PEO-PBD spheres carrying PKH26. (H) Plots of the fluorescence of the cells shown in (G) measured by flow cytometry. *N* = 10 k cells per curve for all plots. All scale bars are 10 μm.

uptake of PEO-PBD filomicelles carrying PKH26 (red) than Idla7 cells that were not expressing SR-BI-GFP (Fig. 4G,H; Fig. S12). Again, no difference was seen in uptake of PEO-PBD spheres carrying PKH26 in these experiments (Fig. 4G,H; Fig. S12).

Since hHDL competes with PEO-PBD filomicelles for SR-BI binding *in vitro*, we wished to determine if hHDL could block or at least diminish PEO-PBD filomicelle uptake *in vivo*. We were particularly interested in any differences in PEO-PBD filomicelle and PEO-PBD sphere localization to the liver, which is the main organ that expresses SR-BI to which NPs

have access. We co-injected (tail-vein) PEO-PBD filomicelles and PEO-PBD spheres carrying near infrared (NIR) dye with unlabeled hHDL. We harvested the major organs and blood 3 h post-injection. We measured the NIR fluorescence of the major organs scaled by organ weight. We observed a \sim 2-fold drop in PEO-PBD filomicelle localization to the livers of wild-type C57BL/6 J mice and a \sim 2-fold increase in PEO-PBD filomicelle presence in the plasma and the gastrointestinal (GI) tract (Fig. 5A,B). Controls were solitary injections of PEO-PBD filomicelles into wild-type C57BL/6 J mice. With PEO-PBD spheres, we observed a

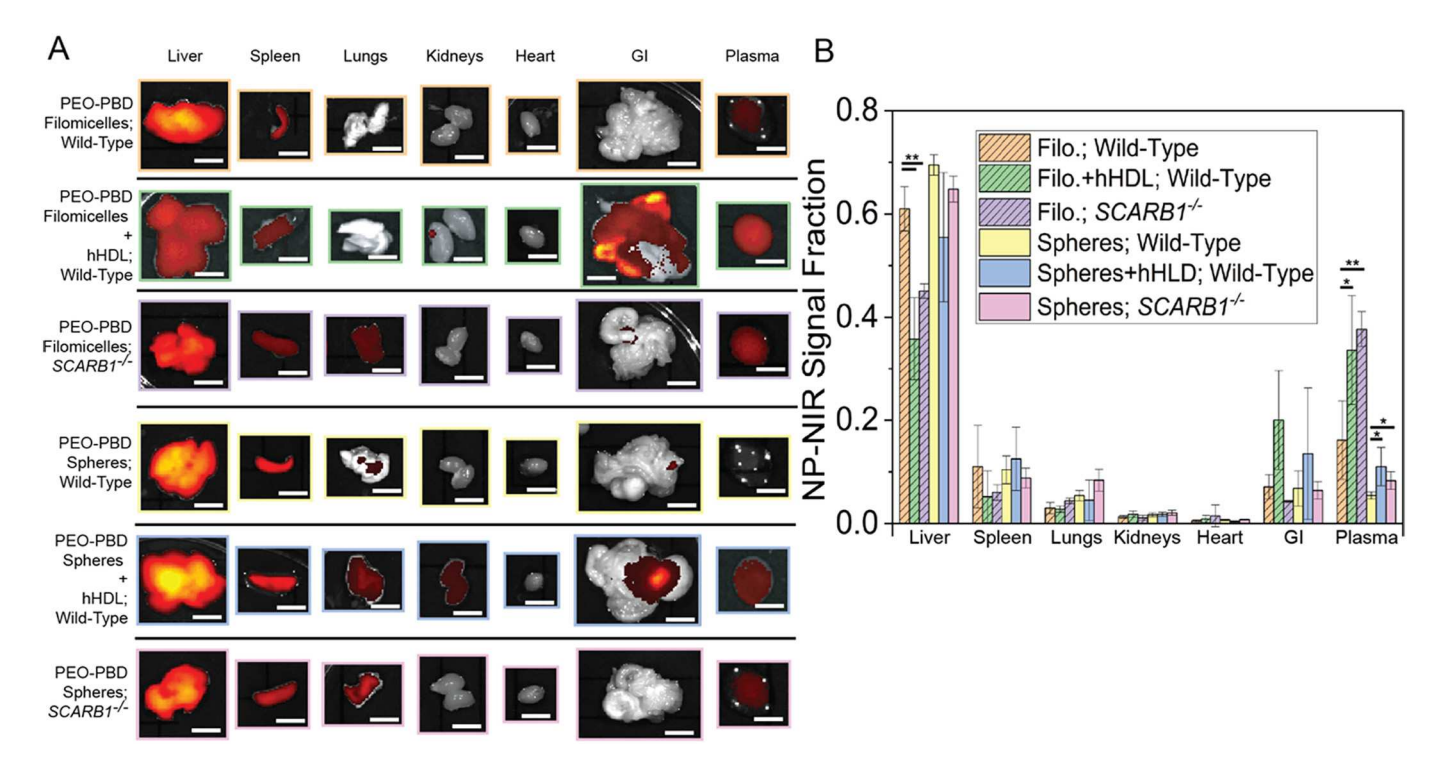


Fig. 5. PEO-PBD filomicelle localization to the liver drops when co-injected with hHDL in wild-type mice and in *SCARB1*-deficient mice when injected solitarily. (A) Fluorescence micrographs of the major organs of wild-type mice that were harvested 3 h post tail-vein injection of either PEO-PBD filomicelles, PEO-PBD filomicelles + hHDL, PEO-PBD spheres, or PEO-PBD spheres + hHDL. The filomicelles and spheres were carrying NIR dye. PEO-PBD filomicelles and PEO-PBD spheres were also administered to $SCARB1^{-/-}$ mice as indicated. Scale bars are 10 mm. (B) Plot of the NIR signal fraction of the organs shown in (A). N=5 mice per bar. * P < 0.1, ** P < 0.05.

slight drop in liver signal between the solitary and co-hHDL injections (Fig. 5A,B). We used $SCARB1^{-/-}$ mice as a model system for mice lacking SR-BI. We repeated the above experiments injecting either PEO-PBD filomicelles or PEO-PBD spheres into the mice. The signal fraction of PEO-PBD filomicelles in the liver dropped ~2-fold from wild-type to $SCARB1^{-/-}$ mice (Fig. 5A,B). There was a corresponding ~2-fold increase in the signal fraction of PEO-PBD filomicelles in the plasma. The signal fraction of PEO-PBD spheres in the liver dropped slightly in $SCARB1^{-/-}$ mice $VCARB1^{-/-}$ mice $VCARB1^{-/-}$ mice $VCARB1^{-/-}$ mice $VCARB1^{-/-}$ mice $VCARB1^{-/-}$ mice. The signal was statistically equivalent across the other major organs between wild-type and $VCARB1^{-/-}$ mice for the spheres (Fig. 5A,B). It is possible that lung monocytes take up PEO-PBD spheres more efficiently than PEO-PBD filomicelles; however, this has not been shown.

We wished to determine if filomicelles were entering macrophages and Idla7-SR-BI cells exclusively through SR-BI or if other factors were involved. We shut down a subset of typical NP entrance pathways using the following inhibitors: colchicine (pinocytosis) [23], cytochalasin B (phagocytosis) [24], rottlerin (macropinocytosis) [25], polyinosinic (PI) acid (lipoprotein endocytosis) [26], and monosdansyl cadaverine (clathrin-mediated endocytosis) [27]. PI acid had no effect on hHDL uptake by M1 and M2 macrophages (Fig. 6A,B; Fig. S13). Only rottlerin had a modest effect on hHDL uptake by M2 macrophages. However, PI acid blocked hHLD uptake by Idla7-SR-BI cells. Cytochalasin B decreased the uptake of filomicelles by M1 and M2 macrophages, whereas PI acid had the strongest effect on decreasing filomicelle uptake by Idla7-SR-BI cells (Fig. 6C,D; Fig. S14). Note the similarity in the uptake profiles of hHDL and filomicelles by M1 and M2 macrophages and Idla7-SR-BI cells when PI acid is used. Fluorescence uptake profiles of spheres by M1 and M2 macrophages showed micropinocytosis being the strongest factor followed by phagocytosis; none of the inhibitors had an effect on sphere uptake by Idla7-SR-BI cells (Fig. 6E,F; Fig. S15). This points to spherical

uptake by Idla7-SR-BI cells being a passive event. PI acid mainly inhibits SR-A [26]. Macrophages express both SR-BI and SR-A [28]. Thus, PI acid is likely binding SR-A on macrophages and SR-BI is still available for binding hHDL, filomicelles, and spheres. Hence, the observed high uptake of hHDL and filomicelles by macrophages in the presence of PI acid (Fig. 6A,B). Therefore, we wished to determine if PI acid inhibits SR-BI in cells with controllable SR-A expression. We transiently transfected Idla7-SR-BI cells, which, unlike macrophages, do not express SR-A (Fig. S16), with mSR-A-GFP. GFP was used to monitor transfection efficiency, not to determine potential co-localization with filomicelles or spheres. Cells expressing mSR-A-GFP took up filomicelles in the presence of PI acid, which should now block mSR-A-GFP instead of SR-BI (Fig. 7A,B; Fig. S17). PI acid has no effect on sphere uptake in these cells (Fig. 7C,D; Fig. S16). This indicates that PI acid can inhibit SR-BI binding to PEO-filomicelles only in the absence of SR-A, its preferred binding partner. Thus, we postulate that filomicelles, like hHDL, bind SR-BI on the surfaces of M1 and M2 murine macrophages.

4. Discussion

PEG/PEO is used in nanomedical applications because it is biocompatible and it has a low affinity for most proteins [29]. Thus, our discovery that PEO-PBD filomicelles have a strong affinity for SR-BI is surprising. However, there are several findings in the literature that foreshadowed our results. PEG-1500 in the crystallization buffer showed electron density in the crystal structure of LIMP-2, a member of the CD36 super family of scavenger receptor proteins, which also includes SR-BI [30]. The Pro270, Thr365, and Lys381 residues near PEG-1500 in the LIMP-2 structure were in the homologous SR-BI cavity/tunnel that is responsible for cholesterol transport [30]. This shows that single PEG/PEO molecules can interact with proteins in the scavenger receptor superfamily. Recently, a crystallography study showed that PEG interacts with anti-PEG Fab at Trp96 of the heavy chain complementarity-

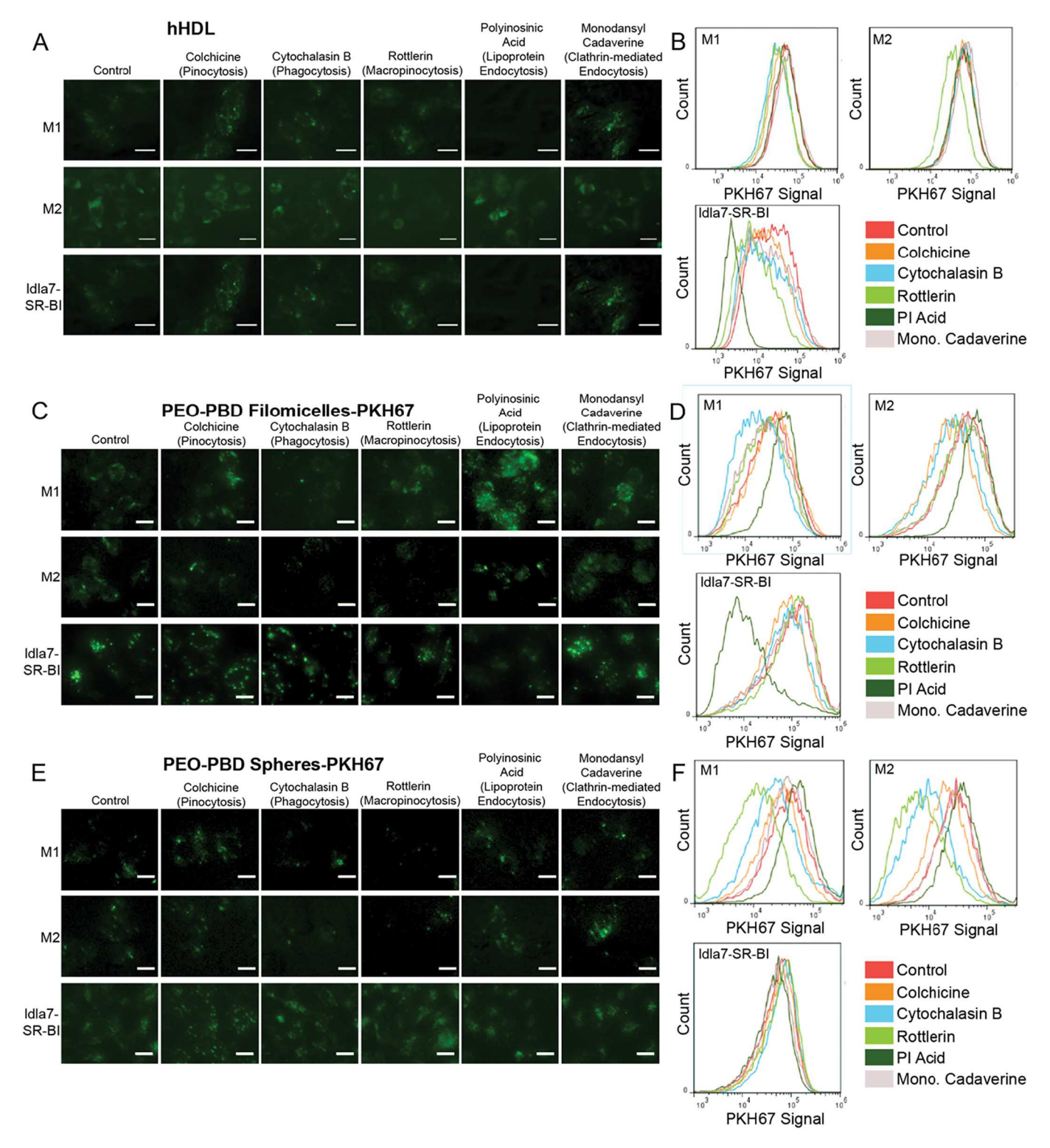


Fig. 6. Entry of hHDL, filomicelles, and spheres into M1 and M2 murine macrophages and Idla7-SR-BI cells. (A) Fluorescence micrographs of M1 and M2 murine macrophages and Idla7-SR-BI cells incubated with hHDL carrying PKH67 and the indicated inhibitors. (B) Plots of the PKH67 fluorescence of the cells shown in (A) measured by flow cytometry. (C) Fluorescence micrographs of M1 and M2 murine macrophages and Idla7-SR-BI cells incubated with PEO-PBD filomicelles carrying PKH67 and the indicated inhibitors. (D) Plots of the PKH67 fluorescence of the cells shown in (C) measured by flow cytometry. (E) Fluorescence micrographs of M1 and M2 murine macrophages and Idla7-SR-BI cells incubated with PEO-PBD spheres carrying PKH67 and the indicated inhibitors. (F) Plots of the PKH67 fluorescence of the cells shown in (E) measured by flow cytometry. N = 10 k cells per curve. All scale bars are 10 µm.

determining region 3 [31]. Trp53, Trp178, and Trp231 are in relatively close proximity to the PEG density in the LIMP-2 structure. They are conserved between LIMP-2 and SR-BI [30]. Given our findings that the affinity of PEG polymers - without PBD - for rSR-BI increases as a

function of PEG length (Fig. 2D), we postulate that PEG may be interacting with these tryptophans in addition to its interaction with the Lys, Pro, and Thr residues listed above. Otherwise, the affinity of PEG for rSR-BI would not be a function of PEG length; each PEG molecule would

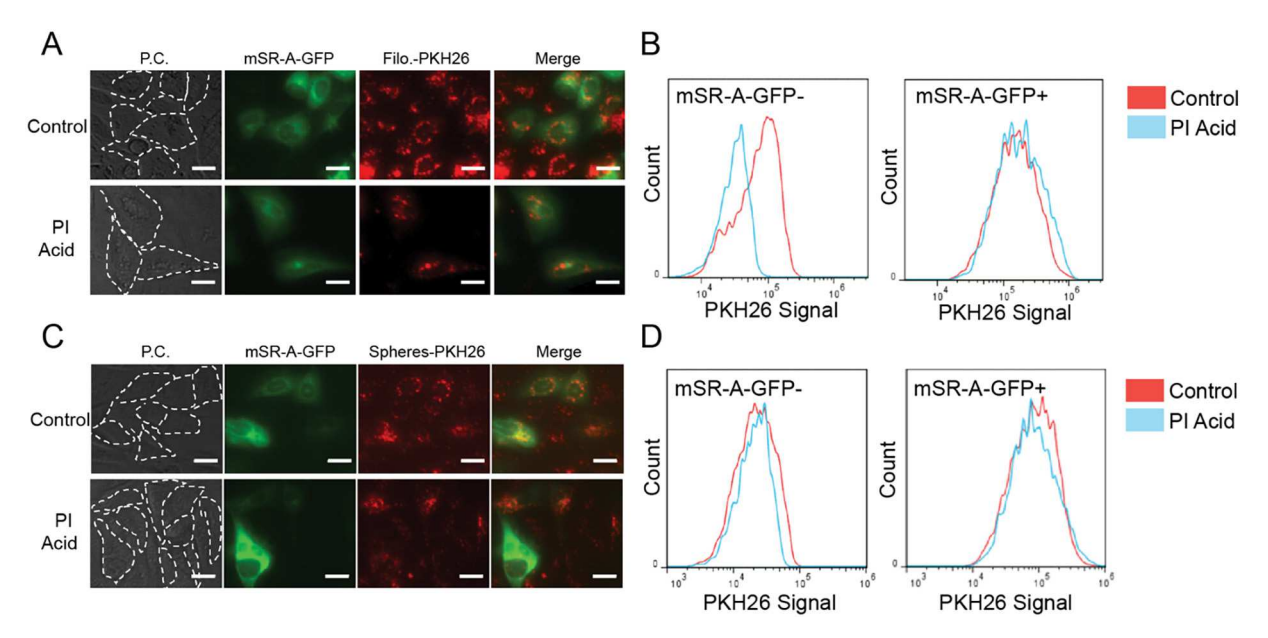


Fig. 7. SR-A does not play a role in PEO-PBD filomicelles uptake by Idla7-SR-BI cells. (A) Fluorescence micrographs of Idla7-SR-BI cells that were transfected with mSR-A-GFP and incubated with PEO-PBD filomicelles-PKH26 with and without PI acid. (B) Plots of the PKH67 fluorescence of the cells shown in (A) measured by flow cytometry. (C) Fluorescence micrographs of Idla7-SR-BI cells that were transfected with mSR-A-GFP and incubated with PEO-PBD spheres-PKH26 with and without PI acid. (D) Plots of the PKH67 fluorescence of the cells shown in (C) measured by flow cytometry. N = 10 k cells per curve. All scale bars are 10 μm.

bind two rSR-BI proteins. This is not what we observe. Additional structural biology and point mutation studies may shed light on the interactions between PEG and protein.

Although our spheres bound rSR-BI, they had weak affinity for cells expressing SR-BI. Spheres bind rSR-BI in pulldowns, but the binding assay showed that spheres have significantly less affinity for rSR-BI than filomicelles. This is further seen by the weak affinity spheres have for cells expressing SR-BI. Filomicelles had consistently stronger interactions with the same cells. We postulate that this is due to cooperativity among a filomicelle and a group of SR-BI receptors on the surface of a cell. HDL could also display cooperativity effects with SR-BI. Nascent HDL particles are disk-shaped molecular aggregates; only after they have taken up cholesterol esters do HDL particles mature into spheres [5]. Thus, HDL have the potential to form elongated Rouleau structures [32]. It is possible that Rouleau HDL particles and filomicelles have binding synergies across multiple SR-BI molecules.

Our results suggest that SR-BI is directly involved in the binding of filomicelles to professional phagocytes and epithelial cells using macrophages and Idla7 as model systems. hHDL and filomicelle entry profiles match in M1, M2, and Idla7-SR-BI cells that are incubated with PI acid. PI acid had no effect on the uptake of hHDL and filomicelles by M1 and M2 macrophages. In contrast, PI acid blocked the uptake of both hHDL and filomicelles by Idla7-SR-BI cells. Macrophages express both SR-BI and SR-A, whereas the Idla7-SR-BI system is not expressing SR-A. PI acid mainly inhibits SR-A [26]. Thus, the addition of PI acid should inhibit SR-A instead of SR-BI in both M1 and M2 macrophages. Therefore, PI acid should have no effect on filomicelle binding and uptake by macrophages because SR-BI should be able to interact with filomicelles even in the presence of PI acid. This also holds for hHDL, as shown. By showing that PI acid does not reduce filomicelle uptake by Idla7 cells coexpressing SR-BI and SR-A-GFP, we confirmed that the SR-BI is still available for filomicelle binding when SR-A is inhibited.

It is not surprising that phagocytosis is the predominant filomicelle entry (but not binding) mechanism in macrophages. Indeed, particle uptake by professional phagocytes involves multiple membrane receptors, cytoskeleton action, bulk membrane flow and remodeling. We postulate SR-BI molecules expressed on macrophages bind filomicelles and bring them in proximity to other receptors that trigger phagocytosis, the main internalization pathway of foreign objects by macrophages.

The identity of these receptors is currently unknown. They could include the Ig receptors FcR and CD14, and/or complement receptor CR3, which binds C3, the only complement factor found on PEGylated liposomes after administration to mice [33].

In the context of NPs, SR-BI is responsible for the importation of HDLcoated silver NPs (AgNPs), and to a lesser extent uncoated AgNPs in RAW 264.7 mouse macrophages [34]. However, it is not clear if this is a direct interaction between AgNPs and SR-BI or if SR-BI controls AgNP uptake indirectly through macrophage activation. By using an epithelial cell line stably expressing SR-BI (Idal7-SR-BI), we were able to study an isolated PEG-SR-BI interaction and avoid effects of macrophage activity. Here we show that this is a direct interaction in the case of filomicelles. Our results point to a strategy to not only target cells expressing SR-BI, but to block the ability of SR-BI expressing phagocytes from clearing elongated PEGylated NPs by co-injection with HDL. Currently, one popular strategy to limit the clearing of NPs is to kill a large fraction of liver resident macrophages - Kupffer cells - using a pre-injection of clodronate liposomes [35]. Naturally, this will compromise the immunity of a potential patient. A strategy of using HDL in place of clodronate liposomes should not put the patient at potential risk because of a weakened immune system. This could be a new approach for extending the circulation and targeting of PEGylated NPs. Additional applications include using filomicelles to block the uptake of pathogens that use SR-BI for cellular entry.

5. Conclusions

We show that by simply elongating a PEGylated NP in one dimension, it has a high affinity for SR-BI. SR-BI is a sought-after target in nanomedical applications from metabolism to virology. Our strategy opens a plethora of options for delivering active agents to cells that express SR-BI.

Supplementary data to this article can be found online at https://doi.org/10.1016/j.jconrel.2021.07.045.

Acknowledgments

The authors thank Dr. Eric Boder for the use of his flow cytometer, Dr. John R. Dunlap for electron microscopy, Deanna Riley for mouse

genotyping, and the Center for Environmental Biotechnology for use of their IVIS imaging system. We also thank Dr. Monty Krieger of MIT for providing Idla7 and Idla7-SR-BI cell lines, Dr. Frank S. Bates of Univ. of Minnesota for diblock copolymers, and Dr. Sergio Grinstein of Univ. of Toronto for the SR-BI-eGFP plasmid. This work was supported in part by the National Institutes of Health R15GM116037.

References

- [1] C.M. Hales, M.D. Carroll, C.D. Fryer, C.L. Ogden, Prevalence of obesity and severe obesity among adults: United States, 2017-2018, NCHS Data Brief 360 (2020).
- S. Acton, et al., Identification of scavenger receptor SR-BI as a high density lipoprotein receptor, Science 271 (1996) 518-520.
- V.N. Sukhorukov, et al., Lipid metabolism: focus on athersclerosis, Biomedicines 8 (2020) 262.
- [4] Y. Ji, et al., Scavenger receptor BI promotes high density lipoprotein-mediated
- cellular cholesterol efflux, J. Biol. Chem. 34 (1997) 20982–30985. [5] K. Frayn, R. Evans, Human Metabolism, 4th edition, Wiley Blackwell, 2019,
- C. Rohrl, H. Stangl, HDL endocytosis and resecretion, Biochem. Biophys. Acta 1831 (2013) 1626-1633
- [7] J. Canton, D. Neculai, S. Grinstein, Scavenger receptors in homeostasis and immunity, Nat. Rev. Immunol. 13 (2013) 621-623.
- [8] M.T. Catanese, et al., Role of scavenger receptor class B type I in hepatitis C virus entry: kinetics and molecular determinants, J. Virol. 84 (2010) 34-43.
- [9] C.C. Colpitts, P.L. Tsai, M.B. Zeisel, Hepatitis C virus entry: an intriguingly complex and highly regulated process, Int. J. Therm. Sci. 21 (2020) 2091.
- [10] C. Wei, et al., SARS-CoV-2 manipulates the SR-BI-mediated HDL uptake pathway for its entry, Nat. Metab. 2 (2020) 1391-1400.
- [11] P. Andre, G. Perlemuter, A. Budkowska, C. Brechot, V. Lotteau, Hepatitis C virus articles and lipoprotein metabolism, Semin. Liver Dis. 25 (2005) 93-104.
- [12] S. Busatto, et al., Lipoprotein-based drug delivery, Adv. Drug Deliv. Rev. 159 (2020) 377-390.
- [13] Y.-Y. Won, H.T. Davis, F.S. Bates, Giant wormlike rubber micelles, Science 283 (1999) 960–963.
- [14] P. Dalhaimer, F.S. Bates, D.E. Discher, Single molecule visualization of stiffness-
- tunable, flow-conforming worm micelles, Macromolecules 36 (2003), 68-73-6877. [15] Y. Geng, et al., Shape effects of filaments versus spherical particles in flow and drug
- delivery, Nat. Nanotechnol. 2 (2007) 249-255.
- [16] S. Zandi, et al., ROCK-isoform-specific polarization of macrophages associated with age-related macular degeneration, Cell Rep. 10 (2015) 1173-1186.
- [17] J.C. Link, et al., Increased high-density lipoprotein cholesterol levels in mice with XX versus XY sex chromosomes, Arterioscler. Thromb. Vasc. Biol. 35 (2015) 1778-1786.

- [18] A.C. Riches, et al., Blood volume determination in the mouse, J. Physiol. 228 (1973) 279-284.
- U.C. Anozie, K.C. Quigley, A. Prescott, S.M. Abel, P. Dalhaimer, Equilibrium binding of isolated and in-plasma high-density lipoprotein (HDL) to polystyrene nanoparticles, J. Nanopart. Res. 22 (2020) 223.
- [20] A. Ji, et al., Scavenger receptor SR-BI in macrophage lipid metabolism, Atherosclerosis 217 (2011) 106–112.
- [21] T.J. Nieland, et al., Discovery of chemical inhibitors of the selective transfer of lipids mediated by the HDL receptor SR-BI, Proc. Natl. Acad. Sci. U. S. A. 99 (2002) 15422-15427.
- [22] K.F. Kozarsky, H.A. Brush, M. Krieger, Unusual forms of low density lipoprotein receptors in hamster cell mutants with defects in the receptor structural gene, J. Cell Biol. 102 (1986) 1567-1575.
- [23] C. Neubauer, A.M. Phelan, H. Kues, D.G. Lange, Microwave irradiation of rats at 2.35 GHZ activates pinocytotic-like uptake of tracer by capillary endothelial cells of cerebral cortex, Bioelectronics 11 (1990) 261-268.
- [24] A.T. Davis, R. Estensen, P.G. Quie, Cytochalasin-B.3. inhibition of human polymorphonuclear leukocyte phagocytosis, Proc. Soc. Exp. Biol. Med. 137 (1971)
- [25] K. Sarkar, M.J. Kruhlak, S.L. Erlandsen, S. Shaw, Selective inhibition by rottlerin of macropinocytosis in monocyte-derived dendritic cells, Immunology 116 (2005)
- [26] R. van Dijk, et al., Polyinosinic acid blocks adeno-associated virus macrophage endocytosis in vitro and enhances adeno-associated virus liver-directed gene therapy, Hum. Gene Ther. 24 (2013) 807-813.
- [27] P.K. Nandi, P.P. van Jaarsveld, R.E. Lippoldt, H. Edelhoch, Effect of basic compounds on the polymerization of clathrin, Biochemistry 20 (1981) 6706-6710.
- V.N. Sukhorukov, et al., Lipid metabolism in macrophages: focus on atherosclerosis, Biomedicines 8 (2020) 262.
- [29] K. Kristenson, T.B. Engle, A. Stensballe, J.B. Simonsen, T.L. Andreson, The hard protein corona of stealth liposomes is sparse, J. Control. Release 307 (2019) 1–15.
- [30] D. Neculai, et al., Structure of LIMP-2 provides functional insights with implications for SR-BI and CD36, Nature 504 (2013) 172-176.
- [31] J.T. Huckaby, et al., Structure of an anti-PEG antibody reveals an open ring that captures highly flexible PEG polymers, Comm. Chem. 3 (2020) 124.
- [32] L. Zhang, et al., Morphology and structure of lipoproteins revealed by an optimized negative-staining protocol of electron microscopy, J. Lipid Res. 52 (2011) 175-194.
- [33] M. Hadjidemetriou, Z. Al-Ahmady, K. Kostarelos, Time-evolution of in vivo protein corona onto blood-circulating PEGylated liposomal doxorubicin (DOXIL) nanoparticles, Nanoscale 8 (2016) 6948-6957.
- [34] A.A. Aldossari, J.H. Shannahan, R. Podila, J.M. Brown, Scavenger receptor B1 facilitates macrophage uptake of silver nanoparticles and cellular activation. J. Nanopart. Res. 17 (2015) 313.
- [35] A.J. Tavares, et al., Effect of removing Kupffer cells on nanoparticle tumor delivery, Proc. Natl. Acad. Sci. U. S. A. 114 (2017) E10871-E10880.